An analytical framework to understand flash drought mechanisms

Vishal Singh[1], Tushar Apurv[1]

Department of Civil Engineering, Indian Institute of Technology, Kanpur, India

Corresponding author: Tushar Apurv (tusharap@iitk.ac.in)

Abstract

Understanding the physical mechanisms which contribute towards the rapid intensification of flash droughts is crucial for improving their forecasts. These mechanisms are difficult to elucidate using statistical techniques due to the complex interactions between land surface and atmospheric processes. In order to overcome this limitation, we use a slab model to model the coupled energy and water balance of the land and atmosphere. We develop an analytical framework to disentangle the influence of external forcings and system response driven by the state variables using the energy and water balance equations of the model. We apply the model to six locations selected from different climate regions of India to identify the physical mechanisms of flash droughts. We find that most flash droughts in India happen during the monsoon season, with higher frequency in humid regions of Northeast India and Southern Peninsular India. We find that all flash droughts occur during periods of deficient rainfall and the drying is predominantly driven by net shortwave radiation. However, the flash droughts differ in terms of contribution of winds towards drying, based on which we classify the flash drought mechanisms into three types: (a) flash droughts with wind-driven intensification due to land-atmospheric feedback (b) flash droughts with minimal contribution of winds towards drying and (c) flash droughts with wind-driven intensification due to advected heat. We also show that although the enhanced vapor pressure deficit is a frequently recurring feature of flash droughts, it is not necessarily the most relevant contributor in their development.

Key words: Flash droughts; Land-atmosphere interaction; Physical mechanisms; Vapor pressure deficit

Key points:

- An analytical framework is proposed to quantify the contributions of external forcings, and system response driven by state variables.
- Shortwave radiation is the major driver of rapid drying of soil during flash droughts in India.
- Vapor pressure deficit increases during flash droughts but is not necessarily a significant contributor in evolution of flash droughts.

1. Introduction

Conventionally, droughts have been referred to as "creeping disasters" due to their gradual development and translation of impacts on the environment and society. However, more rapidly evolving, and intensifying droughts of shorter duration are being observed across the world in recent years (Christian et al., 2021; Yuan et al., 2019), which have been referred to as flash droughts. Apart from having below normal precipitation, these droughts may also be accompanied with above average potential evapotranspiration (E_p) which often quickens depletion of soil moisture (Mahto & Mishra, 2020; Otkin, Svoboda, et al., 2018). The rapid depletion of soil moisture can have disastrous impacts on agriculture, ecology, and economy. For example, the Central United States drought in year 2012 was estimated to cause economic losses of more than 30 billion dollars (Basara et al., 2019). Some other recent flash droughts include the Yangtze River basin drought in the summer of 2022 (Liu et al., 2023), Southeastern Africa drought in 2016 (Quan et al., 2018) and U.S. Northern Plains flash drought in 2016 (Otkin, Haigh, et al., 2018). The complex mechanisms and rapid development of flash droughts pose a significant challenge for their accurate and timely forecasts (Pendergrass et al., 2020).

The term flash drought was first proposed by Svoboda et al. (2002) for describing events with rapid deterioration of crop health due to short spells of intense heat and dryness. Due to the advancements in the understanding of flash droughts, their definitions have been refined and several new indicators have been proposed in the recent years (Lisonbee et al., 2021). Most of these indicators try to identify rapid drying events using precipitation, air temperature, evapotranspiration (ET), and potential evapotranspiration (E_p). Standardized drought indicators like Standardized Precipitation Index (SPI) and Standardised Precipitation-evapotranspiration Index (SPEI), which have been traditionally used for quantification of long-term droughts, have also been used for flash drought identification by calculating them at 5-10 day intervals (Hunt et al., 2014; Noguera et al., 2021). Indices based on ET and E_p include the Evaporative Demand Drought Index (EDDI; Hobbins et al., 2016), Evaporative Stress Index (ESI; Anderson et al., 2007; Otkin et al., 2013) and Standardized Evaporative Stress Ratio (SESR; Christian et al., 2021; Gong et al., 2022). Several studies have used the rapid changes in United Sates Drought Monitor (USDM) drought categories as a criterion for the identification of flash droughts (Chen et al., 2019; Lorenz et al., 2017; Otkin et al., 2013; Pendergrass et al., 2020). Rapid declines in soil moisture (SM) percentiles have also been used for identifying flash droughts in some studies (Han et al., 2023; Mahto & Mishra, 2020a; Y. Wang & Yuan, 2022; Yuan et al., 2019). Otkin et al., (2021) has recently developed soil moisture percentile-based Flash Drought Intensity Index (FDII) which takes both rapid intensification and drought severity into account.

Significant advances have also been made in understanding the mechanisms of flash droughts. Wang & Yuan (2018) found that in humid regions like Southern China, elevated temperatures combined with high antecedent soil moisture can lead to rapid drying through enhanced ET whereas in semi-arid Northern China, flash droughts are driven by precipitation deficits. Similarly, Mo & Lettenmaier (2015), showed that flash droughts in the Conterminous United States

(CONUS) can be classified into two categories: first, which are driven by enhanced elevated temperature and increased ET (heat wave flash droughts) and those which are driven by precipitation deficits (precipitation deficit flash droughts). They further showed that precipitation-driven flash droughts are twice as frequent as ET-driven flash droughts over the CONUS (Mo & Lettenmaier, 2016). Otkin et al., (2013) and Parker et al., (2021) showed that E_p based indices like ESI can predict flash drought onset better than precipitation indices in Southeast Australia and United States respectively. Strengthening this hypothesis, Chen et al. (2019) showed that ET-related processes constitute the major driving mechanisms of flash drought intensification in the CONUS. Osman et al. (2022) classified flash drought events based on antecedent hydrometeorological conditions into three categories: (1) flash droughts with high antecedent E_p and low SM, (2) flash droughts with high antecedent E_p and moderate SM and (3) flash droughts with modest anomalies of antecedent E_p and SM. At the global scale, precipitation deficit has been shown to be the dominant contributor to flash droughts (Hoffmann et al., 2021; Koster et al., 2019). These results indicate that the driving mechanisms of flash droughts can vary considerably seasonally across regions.

In several recent studies, the role of land-atmospheric interactions in flash drought intensification has also received significant attention (Miralles et al., 2019). Ahmad et al., (2022) found that decrease in soil moisture contributed to positive feedback between increased atmospheric temperature and sensible heating, that accelerated the rate of drying of soil. Qing et al., (2022) analysed the rate of intensification of flash droughts globally and showed that the coupling between SM and vapor pressure deficit (VPD) contributes significantly to rapid intensification of flash droughts. Wang & Yuan (2022) showed that increased LA-coupling during flash droughts, i.e., the positive feedback between increased sensible heat and atmospheric temperature, accelerates the rate of drying of soil over Southern China.

India has been found to be one of the global hotspots of flash drought occurrence (Christian et al., 2021, 2023), with majority of them occurring during the monsoon season (Mahto & Mishra, 2020, 2023; Mishra et al., 2021). The frequency of flash droughts in India is expected to increase multi-fold in near future due to climate change (Mishra et al., 2021). Being an agriculture-based economy, where 68 percent of population is involved in farming or allied sectors (Chandra & Malaya, 2011; Dhawan, 2017; Joshi, 2015), flash droughts pose a significant threat both to food security and economy. The flash droughts in India have been attributed to increased air temperature and below normal precipitation (Christian et al., 2021; Mahto & Mishra, 2020), which are exacerbated by land-atmospheric interactions (Mishra et al., 2021). Flash droughts in Northeast and Peninsular India have been found to be associated with high SM-VPD coupling (Mahto & Mishra, 2023). In a recent work, Das et al. (2023) show that anomalies in surface latent and sensible heat flux act as the triggers for flash drought onset in India.

Most of the above-mentioned studies have used statistical methods for deciphering the physical mechanisms of flash droughts by either analysing anomalies of hydrometeorological variables

during and before flash droughts (Mo & Lettenmaier, 2015; Wang & Yuan 2018; Koster et al. 2019; Osman et al., 2022), using correlation analysis (Qing et al., 2022; Mahto & Mishra, 2023) or using flash drought indicators based on different hydrometeorological variables (Otkin et al. 2013; Parker et al. 2021; Hoffmann et al., 2021; Das et al., 2023). A major limitation of using statistical methods for studying land-atmospheric interactions is that the co-variability of variables might not actually imply a causal relation between them due to the strong coupling of land and atmospheric processes (Orlowsky & Seneviratne, 2010). For instance, the air temperature can increase during droughts due to solar radiation, sensible heat flux as well as advected heat flux. Thus, a positive anomaly of solar radiation during a drought may not mean that the rise in air temperature is caused by solar radiation. Furthermore, the rapid drying during flash droughts represents the combined effect of anomaly in external forcings such as wind, precipitation and radiation, and the system response through land-atmospheric interactions, which cannot be distinguished using statistical methods. Quantifying the contributions of external forcings and system response to flash droughts is critical for understanding their physical mechanisms and improving their predictability. While researchers have developed frameworks for attributing the changes in E_p to its meteorological and radiative drivers (Hobbins, 2016), such a framework has not been developed for attributing the rapid decline in soil moisture during flash droughts.

In this study, we use an analytical model developed by Brubaker & Entekhabi (1995; referred to as BE95 in this paper) for understanding the physical mechanisms of flash droughts. The BE95 model simulates the land-atmospheric interactions by representing the atmosphere as a single slab of fixed height and the land surface as a single layer of soil. The model includes four state variables (soil moisture (s), specific humidity (q_m), ground temperature (t_g) and atmospheric temperature (θ_m)), which are computed by solving the energy and water balance equations. While Brubaker & Entekhabi, (1995) used the model to analyse the effect of land-atmospheric interaction on the long-term regional climate, we apply this model for understanding flash drought mechanisms. We use forcings derived from reanalysis datasets to run the BE95 model in six locations in India which are representative of the different climate regimes across the country. We use the water and energy balance equations of the model to develop an analytical framework for segregating the effects of external forcings and response induced by the state variables on soil moisture declines during flash droughts.

The remainder of this paper is organized as follows: section 2 provides a description of the BE95 model, the proposed framework to decompose changes in state variables due to external forcings and system-driven changes, datasets used and the study regions. The validation of the model and the three identified flash drought mechanisms are described in section 3. Section 4 provides discussion on the seasonal and regional variation of flash drought characteristics, comparison of findings with previous studies and limitations of the study. Section 5 concludes the paper with the major findings of the study.

2. Methodology

In section 2.1, we first describe the equations which are solved in the BE95 model. The parameters and forcing variables used for running the model are discussed in section 2.2. In section 2.3, we describe how we use the water and energy balance equations of the model to quantify the contributions of external forcings and system response to flash drought evolution. Section 2.4 provides the details of the locations selected for the analysis of flash droughts.

2.1 The BE95 model

The BE95 model is a lumped model with two reservoirs: one representing the mixed layer of the atmosphere and the other representing the top ground layer. The lumped representation of land and atmosphere in the model implies that the state variables are assumed to be invariant with respect to height of the atmospheric mixed layer and depth of ground. The model also assumes that the height of the mixed layer does not vary with time. The model has four state variables: specific humidity ($q_m[-]$), atmospheric temperature ($\theta_m[\mathrm{K}]$), relative soil moisture ($s[-]$) and ground temperature ($t_g[\mathrm{K}]$), which are calculated by solving the energy and water balance equations for land and atmosphere reservoirs:

$$\frac{d}{dt}\begin{bmatrix} s \\ q_m \\ t_g \\ \theta_m \end{bmatrix} = \begin{bmatrix} \dfrac{P-R-ET}{\rho_w z_h}, & (1a) \\ \dfrac{ET}{\rho h} + S_{q_{adv.}} \times (Q_{in}-Q_{out}) - Q_{top} - P_p \times q_m, & (1b) \\ \dfrac{R_{ns} - RL_{gu} + RL_{sd} + C_{t_g}(1-\epsilon_m)RL_{ad} - H - \lambda ET}{z_t C_{sV}}, & (1c) \\ \dfrac{\epsilon_m(RL_{gu}+RL_{ad}) - RL_{sd} - RL_{su} + H + H_{top}}{\rho c_p h} + S_{\theta_{adv.}} \times (H_{in}-H_{out}) & (1d) \end{bmatrix}$$

Equation (1a) in the above matrix describes water balance at the ground surface. The change in soil moisture is the residual of precipitation P and the sum of runoff R and evapotranspiration ET, where ρ_w denotes the density of water and z_h denotes the hydrologically active soil depth, which contributes to runoff and evapotranspiration. Runoff is modelled as a product of precipitation and a non-linear function of soil moisture with parameters η and r.

$$\boldsymbol{R = \eta P s^r} \quad (2)$$

Evapotranspiration from soil (ET) is calculated as a product of potential evapotranspiration (E_p) and evaporation efficiency ($\beta(=s^c)$), which decreases as the soil dries. We calculate E_p using the simplified FAO Penman-Monteith (PM) equation, which includes two components driven by: 1) radiation and 2) turbulent moisture transfer through wind.

$$ET = \beta E_p = \beta(E_{p_{rad}} + E_{p_{wind}}) \quad (3)$$

in which $E_{p_{rad}} = 0.408 R_n b_1$, where R_n $(= R_{ns} - RL_{gu} + RL_{sd} + (1 - \epsilon_m)RL_{ad})$ is the net radiation at the ground surface, R_{ns} is the net shortwave radiation on the ground surface after subtracting the shortwave radiation reflected due to albedo, RL_{gu} is the longwave radiation emitted by the ground upwards, ϵ_m is the emissivity of the atmospheric mixed layer, and RL_{sd} and RL_{ad} are the longwave radiation incident at the ground surface from within the mixed layer and top of the mixed layer respectively. The term $b_1 \left(= \frac{\Delta}{\Delta+\gamma}\right)$ is the ratio of slope of the temperature-saturation vapor pressure relation (Δ) to the sum of Δ and psychrometric constant (γ). RL_{ad} is calculated using the air temperature at the top of the mixed layer θ_{m_a}, which is related to the mixed layer temperature θ_m through the following relation:

$$\theta_{m_a} = \theta_m \left(\frac{P_h}{P_s}\right)^{\left(\frac{R_d}{c_p}\right)} \quad (4)$$

where P_h and P_s are the atmospheric pressure at the top and bottom of the mixed layer respectively, R_d is the gas constant for dry air and c_P is the dry air specific heat at constant pressure.

$E_{p_{wind}}$ in equation 3 is the product of three terms $b_2 \left(= \frac{\gamma}{\Delta+\gamma}\right)$, $b_3 \left(= \frac{900}{\theta_m} u_2\right)$ and $b_4 (= e_s - e_a)$, in which u_2 is the wind velocity at 2m height form the surface and e_s and e_a are the saturated and actual vapor pressure respectively. The term b_4 is the vapor pressure deficit (VPD). The slope of temperature-saturation vapour pressure relationship is given by:

$$\Delta = \frac{4098 \times e_s}{(\theta_m + 237.3)^2} \quad (5)$$

And the saturation vapor pressure (e_s) is calculated as:

$$e_s = 0.6108 \times e^{\frac{17.27 \times \theta_m}{\theta_m + 237}} \quad (6)$$

Equation (1b) in the matrix represents the moisture balance in the atmospheric reservoir. There are two sources of moisture for the atmospheric reservoir: evapotranspiration from the ground surface and the advected moisture (Q_{in}). Out of total moisture available in atmospheric mixed layer, a fraction (P_p) is assumed to precipitate. The reservoir can lose moisture through air advected out of the reservoir (Q_{out}) and dry air entrainment from the top of the mixed layer (Q_{top}), which is assumed to be zero for simplicity. $(Q_{in}[-])$ and $(Q_{out}[-])$ represent the change in specific humidity of the atmosphere due to advection of incoming and outgoing moisture, which is calculated as the advected mass flux of water vapour divided by the mass of air column. In this study, we adjust the humidity advection term by a factor $S_{q_{adv.}}$ to match the ERA5 specific humidity time series.

Equation (1c) in the matrix represents energy balance of the ground surface. The ground surface receives energy from net shortwave radiation (R_{ns}), longwave radiation from the mixed layer (RL_{sd}) and top of the mixed layer (RL_{ad}) and loses energy through longwave radiation emitted by the ground $\left(RL_{gu}\right)$, sensible heat flux (H) and latent heat flux (λE). We found that RL_{ad} calculated using the Stefan-Boltzmann Law led to overestimation of ground temperature when compared to the ERA5 ground temperature time series. Hence, we used a coefficient C_{t_g} to adjust RL_{ad} and reduce the bias. The sensible heat flux is calculated as:

$$H = C_{HE}\left(t_g - \theta_m\right)\rho c_p \tag{7}$$

where $C_{HE}(= 86400 c_1 u_2)$ is the coefficient of transfer of heat, in which c_1 is the coefficient of sensible heat and ρ is the density of air. In equation 1c, C_{sV} is the volumetric heat capacity of the soil and z_t is thermally active soil depth which actively exchanges energy with the atmosphere. We estimate C_{sV} using the following formula (Huang et al., 2011).

$$C_{sV} = \frac{2.0 \times 10^6}{2.65}\mathrm{B}D_{soil} + 4.2 \times 10^6 s_{avg} + 2.5 \times 10^6 \mathrm{SO}M_v \tag{8}$$

where bulk density of soil (BD_{soil}) and organic matter content of soil (SOM_v) are based on data from Harmonised World Soil Database (HWSD). s_{avg} is the average moisture for the soil.

Equation (1d) in the matrix represents energy balance of the atmospheric reservoir. The reservoir receives energy from longwave radiation emitted by the ground surface $\left(RL_{gu}\right)$ and the top of the atmosphere (RL_{ad}), sensible heat emitted by ground surface (H) and heat entrained from top of the atmosphere (H_{top}), which is assumed to be 20% of H. The atmospheric reservoir loses energy through the longwave radiation emitted in the upward (RL_{su}) and downward (RL_{sd}) directions. The terms ($H_{in}[K]$) and (H_{out}[K]) represent the change in temperature of the mixed layer due to the heat flux advected in and out of the atmosphere respectively and are calculated as the advected heat flux divided by the mass of air and specific heat capacity of air in the reservoir. The heat advection terms are adjusted by a factor $\left(\mathrm{S}_{\theta_{\mathrm{adv.}}}\right)$ to match the ERA5 atmospheric temperature time series.

The longwave radiation terms are calculated using the Stefan-Boltzmann law as $RL_{gu} = \epsilon_s \sigma t_g^4$; $RL_{sd} = \epsilon_m \sigma \theta_m^4$; $RL_{su} = \epsilon_m \sigma \theta_m^4$ and $RL_{ad} = \epsilon_a \sigma \theta_{m_a}^4$ respectively, where ϵ_s is the emissivity of the soil and ϵ_a is the emissivity of the top of the atmosphere.

Brubaker & Entekhabi, (1995) reported that BE95 model works well in partitioning the incoming shortwave radiation into latent and sensible heat. Entekhabi & Brubaker (1995) later used this model to study the influence of energy-water coupling in determining different states of the land atmosphere system. In this study, we have made two major modifications to the BE95 model. Firstly, we consider precipitation as an external forcing to the model, while precipitation was

modelled as a function of the atmospheric humidity in the original BE95 model. This change was required since flash drought occurrence is highly sensitive to daily rainfall deficits which cannot be captured by the simplified relations used in the original model. Secondly, we use the Penman-Montieth equation for modelling potential evapotranspiration, which is better suited for quantifying the contribution of shortwave radiation and winds towards rapid depletion of soil moisture as compared to the simplified relation used in the original BE95 model. Hereafter, we refer to the modified model as MBE95 model.

2.2 Forcing datasets and parameters

The MBE95 model was run for 30 years (1992-2021) at the daily scale. The forcing data required to run the model were taken from the ERA5 climate reanalysis dataset (Hersbach et al., 2020) produced by European centre for medium range weather forecast (ECMWEF) which is available at open access from Copernicus climate data store (CDS). This dataset consists of gridded global climate reanalysis outputs on $0.25^0 \times 0.25^0$ regular latitude-longitude grids available at hourly scale. The data was downloaded at 4-hour intervals and aggregated to daily scale. The following forcing variables are used to run the model: 1) net shortwave radiation at ground surface, 2) precipitation, 3) incoming advected moisture, 4) outgoing advected moisture, 5) incoming advected heat, 6) outgoing advected heat, and 7) 10m wind velocity. Wind velocity at pressure levels of 875 and 950 hPa in the reanalysis dataset were used in the calculation of heat and moisture advection into the mixed layer. We converted the 10m wind velocity from the reanalysis dataset to 2m wind velocity, required for calculating potential evapotranspiration, using the following relation (Allen et al., 1998).

$$u_2 = 0.748(u_{10}) \tag{9}$$

Other than the forcing variables, the model requires some parameters and constants which need to be specified. We used soil moisture, ground temperature, atmospheric temperature, and specific humidity from the ERA5 dataset to manually calibrate the model parameters. The following parameters were calibrated manually: emissivity of the soil (ϵ_s), emissivity of the top of the atmosphere (ϵ_a) , coefficient for energy balance at ground surface (C_{t_g}), factor for moisture adjustment in the atmosphere (P_p), factors for adjustment of advected moisture $\left(\mathrm{S}_{\mathrm{q}_{\mathrm{adv.}}}\right)$ and advected heat $\left(\mathrm{S}_{\theta_{\mathrm{adv.}}}\right)$. These parameters were adjusted by trial-and-error to match the simulated state variable time series with the ERA5 time series for that variable. Volumetric heat capacity of soil (C_{sV}) was calculated using equation 8. Height of the atmospheric mixed layer (h) is fixed to 988.5m which corresponds to the height of the lowest atmospheric layer in the ERA5 dataset. Emissivity of the atmospheric mixed layer ($\epsilon_m = 0.56$) is fixed. Thermally active soil depth (z_t) and hydrologically active soil depth (z_h) are fixed to be 1 m each. The calibrated parameters are presented in Table 1 in the results section.

2.3 Quantification of role of external forcings and system response

We segregated the changes in the state variables $\mathbf{X_t}$ on the day t into those caused by the initial state of the system $\mathbf{G(X_t)}$ and those driven by external forcings $\mathbf{H}$. The change produced by external forcings is the product of external forcings $\mathbf{F_t}$ and the sensitivity of the system to external forcings which is a function of the state variables $\mathbf{g(X_t)}$.

$$\frac{d\mathbf{X_t}}{dt} = \mathbf{G(X_t)} + \ \mathbf{H(X_t, F_t)} \tag{10}$$

$$\mathbf{H(X_t, F_t)} = \mathbf{g(X_t)}.\mathbf{F_t} \tag{11}$$

In the remaining text, we drop the notation t to simplify the expressions. In the above equation, $\mathbf{G(X_t)}$ is the vector function whose elements are G^s, G^{q_m}, G^{t_g} and G^{θ_m} representing the changes in soil moisture, humidity, ground temperature and air temperature respectively, which are driven by the systems response.

$$\mathbf{G(X)} = \begin{bmatrix} G^s \\ G^{q_m} \\ G^{t_g} \\ G^{\theta_m} \end{bmatrix}$$

$$= \begin{bmatrix} -\dfrac{0.408\frac{\Delta}{\Delta+\gamma}\beta\left(RL_{sd} - RL_{gu} + (1-\epsilon_m)RL_{ad}\right)}{\rho_w z_h}, & \text{(12a)} \\ \dfrac{0.408\frac{\Delta}{\Delta+\gamma}\beta\left(RL_{sd} - RL_{gu} + (1-\epsilon_m)RL_{ad}\right)}{\rho h} - P_p \times q_m, & \text{(12b)} \\ \dfrac{RL_{sd} - RL_{gu} + C_{t_g}(1-\epsilon_m)RL_{ad}}{z_t \mathrm{C_{sV}}} + \dfrac{0.408\frac{\Delta}{\Delta+\gamma}\beta\lambda\left(RL_{gu} - RL_{sd} - (1-\epsilon_m)RL_{ad}\right)}{z_t \mathrm{C_{sV}}}, & \text{(12c)} \\ \dfrac{\left(RL_{gu} + RL_{ad}\right)\epsilon_m - RL_{sd} - RL_{su}}{\rho h c_p} & \text{(12d)} \end{bmatrix}$$

The forcing vector consists of seven variables:

$$\mathbf{F} = \left[P_t, u_{2_t}, Q_{in_t}, Q_{out_t}, H_{in_t}, H_{out_t}, R_{ns_t}\right]^{\mathrm{T}} \tag{13}$$

The elements of the sensitivity matrix g^{i_j} represent the sensitivity of the i^{th} state variable to the j^{th} forcing variable.

$$\mathbf{g(X)} = \begin{bmatrix} g^s \\ g^{q_m} \\ g^{t_g} \\ g^{\theta_m} \end{bmatrix} = \begin{bmatrix} g^{s\_P} & g^{s\_u_2} & g^{s\_Q_{in}} & g^{s\_Q_{out}} & g^{s\_H_{in}} & g^{s\_H_{out}} & g^{s\_R_{ns}} \\ g^{q_m\_P} & g^{q_m\_u_2} & g^{q_m\_Q_{in}} & g^{q_m\_Q_{out}} & g^{q_m\_H_{in}} & g^{q_m\_H_{out}} & g^{q_m\_R_{ns}} \\ g^{t_g\_P} & g^{t_g\_u_2} & g^{t_g\_Q_{in}} & g^{t_g\_Q_{out}} & g^{t_g\_H_{in}} & g^{t_g\_H_{out}} & g^{t_g\_R_{ns}} \\ g^{\theta_m\_P} & g^{\theta_m\_u_2} & g^{\theta_m\_Q_{in}} & g^{\theta_m\_Q_{out}} & g^{\theta_m\_H_{in}} & g^{\theta_m\_H_{out}} & g^{\theta_m\_R_{ns}} \end{bmatrix} \tag{14}$$

The terms of the sensitivity matrix for soil moisture are obtained from the soil water balance equation 1a. Sensitivity of soil moisture with respect to precipitation is obtained from equation 1a and equation 2 as:

$$g^{s\_P} = \frac{(1 - \eta s^r)}{\rho_w z_h} \tag{15}$$

which means that as the soil moisture decreases, its sensitivity to precipitation increases because when the soil moisture level is low, the evaporation and runoff rates are lower. Similarly, sensitivity of soil moisture with respect to wind and shortwave radiation are obtained using PM equation as

$$g^{s\_u_2} = -\frac{\beta \frac{\gamma}{\Delta + \gamma}(e_s - e_a)\left(\frac{900}{\theta_m}\right)}{\rho_w z_h} \tag{16}$$

which implies that as VPD increases, the sensitivity of soil moisture to wind velocity increases due to increase in potential evapotranspiration at higher VPD.

$$g^{s\_R_{ns}} = -\frac{0.408\beta b_1}{\rho_w z_h} \tag{17}$$

Equation 17 implies that if $\beta(= s^c)$ or $b1$ have high anomaly, the rate of decline of soil moisture due to shortwave radiation will be high. The sensitivity of soil moisture to other external forcings are zero ($g^{s\_Q_{in}} = 0; g^{s\_Q_{out}} = 0; g^{s\_H_{in}} = 0; g^{s\_H_{out}} = 0$).

The sensitivity of specific humidity with respect to forcings are calculated from the moisture balance equation of the atmosphere (equation 1b). The sensitivity of specific humidity to wind and shortwave radiation is calculated from the evapotranspiration equation (equation 3):

$$g^{q_m\_u_2} = \frac{\beta(e_s - e_a)\frac{\gamma}{\Delta + \gamma}\left(\frac{900}{\theta_m}\right)}{\rho h} \tag{18}$$

$$g^{q_m\_R_{ns}} = \frac{0.408\beta \frac{\Delta}{\Delta + \gamma}}{\rho h} \tag{19}$$

The other sensitivity terms are $g^{q_m\_P} = 0; g^{q_m\_Q_{in}} = \mathrm{S}_{\mathrm{q_{adv.}}}; g^{q_m\_Q_{out}} = -\mathrm{S}_{\mathrm{q_{adv.}}}; g^{q_m\_H_{in}} = 0;\ g^{q_m\_H_{out}} = 0$.

Ground temperature is influenced by wind velocity through sensible heat flux and latent flux. Therefore, the sensitivity of ground temperature with respect to wind velocity can be calculated by combining equations 1c, 3 and 7.

$$g^{t_g\_u_2} = -\frac{C_{HE}(t_g - \theta_m)\rho c_p}{z_t C_{pv}} - \frac{\beta\lambda(e_s - e_a)\frac{\gamma}{\Delta+\gamma}\left(\frac{900}{\theta_m}\right)}{z_t C_{pv}} \quad (20)$$

$$g^{t_g\_R_{ns}} = \frac{10^6 - 0.408\beta\lambda\frac{\Delta}{\Delta+\gamma}}{z_t C_{pv}} \quad (21)$$

Shortwave radiation affects ground temperature directly as well as through evapotranspiration (Equation 1c). Therefore, its sensitivity is given by equation 21. The value 10^6 in the numerator comes due to conversion of shortwave radiation from Megajoule to Joule.

Other sensitivity terms for ground temperature are $g^{t_g\_P} = 0$; $g^{t_g\_Q_{in}} = 0$; $g^{t_g\_Q_{out}} = 0$; $g^{t_g\_H_{in}} = 0$; $g^{t_g\_H_{out}} = 0$.

Wind affects atmospheric temperature through sensible heat flux. Therefore, the sensitivity with respect to wind is calculated by combining the energy balance of atmosphere (equation 1d) and the sensible heat equation (equation 7):

$$g^{\theta_m\_u_2} = \frac{1.2C_{HE}(t_g - \theta_m)\rho c_p}{\rho h c_p} \quad (22)$$

The other sensitivities of atmospheric temperature are $g^{\theta_m\_P} = 0$; $g^{\theta_m\_Q_{in}} = 0$; $g^{\theta_m\_Q_{out}} = 0$; $g^{\theta_m\_H_{in}} = S_{\theta_{adv.}}$; $g^{\theta_m\_H_{out}} = -S_{\theta_{adv.}}$; $g^{\theta_m\_R_{ns}} = 0$.

2.4 Study locations

In order to analyse the flash drought mechanisms in different regions of India, we consider representative locations from each of the six homogenous precipitation regions defined by the Indian Meteorological Department (IMD; shown in Figure 1): Western Central (WC), South Peninsular (SP), Northeast (NE), Hilly Regions (HR), Central Northeast (CNE) and Northwest (NW). We run the MBE95 model with the forcing variables for these locations derived from the ERA5 dataset.

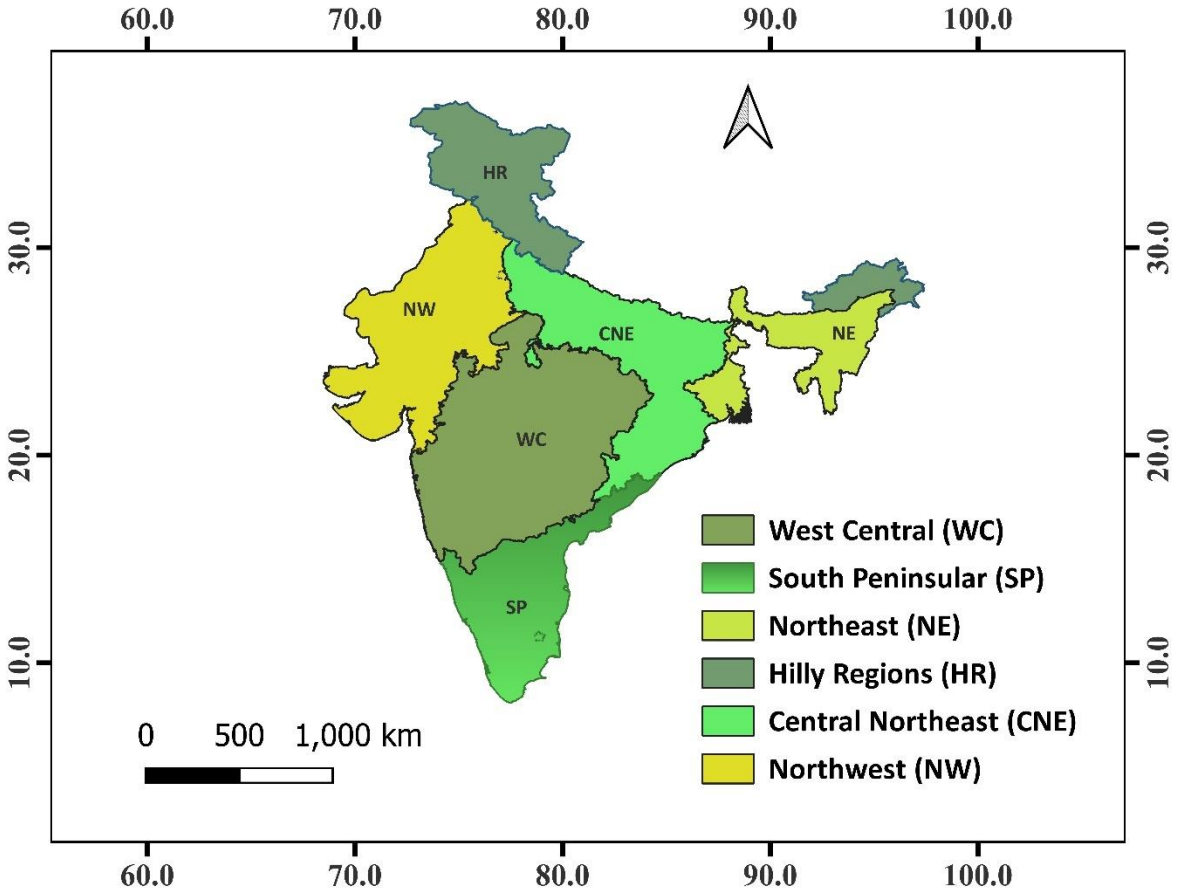

Figure 1 Indian Meteorological Department (IMD) homogenous precipitation regions. IMD has mapped India into six different precipitation regimes based on spatial distribution of rainfall patterns.

3. Results

3.1 Model parameters

The MBE95 model has 13 parameters. Five of the parameter values are taken from the study by Brubaker & Entekhabi (1995) and are provided in the appendix section. Average elevation of different places (h) are taken from google maps. Rest of the parameters have been calibrated manually. Table 1 enlists the values of the calibrated parameters for each region.

Table 1 Calibrated parameters for each region

Parameter	NE (h = 59 m)	HR (h = 763 m)	CNE (h = 126 m)	PR (h = 84 m)	WC (h = 491 m)	NW (h = 221 m)
ϵ_s	0.96	1	1	1	1	1
C_{t_g}	0.66	0.50	0.80	0.57	0.65	0.69
ϵ_a	0.90	0.85	0.81	0.85	0.80	0.79
P_p	0.21	0.15	0.16	0.18	0.18	0.13
C_{pv}	2.49×10^6	2.35×10^6	2.27×10^6	2.89×10^6	2.76×10^6	1.98×10^6
$S_{\theta_{\text{adv.}}}$	0.14	0.52	0.10	0.09	0.13	0.15
$S_{q_{\text{adv.}}}$	0.12	0.41	0.07	0.18	0.14	0.15

ϵ_s = Emissivity of soil, C_{t_g} = Coefficient for energy balance at ground surface, ϵ_a = Emissivity of atmosphere, P_p = Coefficient for moisture balance in atmosphere, C_{pv} = Volumetric heat capacity of soil, $S_{\theta_{\text{adv.}}}$ = Scaling for advected heat, $S_{q_{\text{adv.}}}$ = Scaling for advected moisture

3.2 Model validation

Figure 2 illustrates the comparison of the model-simulated standardized soil moisture anomalies with those from the ERA5 dataset up to a depth of 1 m at the pentad-scale. The anomalies are calculated as the difference between the value of the state variable and the climatological mean divided by the standard deviation for that pentad. A soil depth of 1 m corresponds to the total of first, second and third layer of soil in the ERA5 reanalysis dataset. The model seems to be in good agreement with the ERA5 soil moisture time-series. In conjunction with our objective of deciphering flash drought mechanisms using an analytically tractable model, the results suggest that the model is capable of capturing the soil moisture variability in the ERA5 dataset. We also found that the model was able to reasonably reproduce the variability of ground temperature, mixed layer temperature, and specific humidity (Figures S1-S3 in the supporting information).

In accordance with the existing literature (Ford & Labosier, 2017; Mahto & Mishra, 2020b), we define flash droughts as periods in which soil moisture decreases from above 40th percentile to below 20th percentile within a predefined threshold number of pentads, which is region-specific. Since the climate characteristics vary significantly across the 6 precipitation regions, the use of same threshold for maximum number of pentads resulted in identification of a very small number of flash droughts in some regions. Therefore, we set the threshold of 5 pentads for NE, CNE, SP and NW and 7 pentads for HR and WC as the maximum number of pentads in which soil moisture should fall from above 40^{th} percentile to below 20^{th} percentile to be classified as a flash drought. We observed that the frequency of flash droughts varies across India with higher frequency in the humid regions of NE and PR. Within the observation period of 30 years, we identified 19 flash droughts in NE, 18 in HR, 11 in CNE, 36 in SP, 15 in WC and 9 in NW regions.

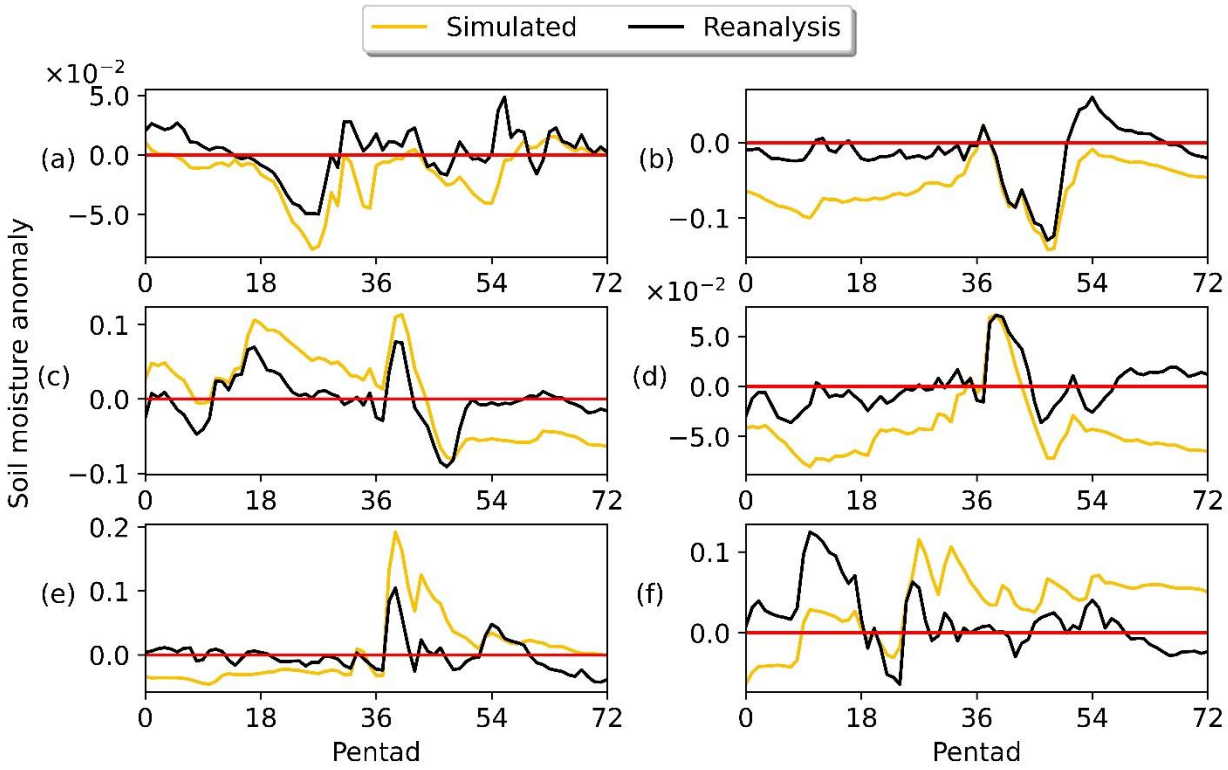

Figure 2 Comparison of pentad-scale model-simulated (yellow) and ERA5(black) standardized soil moisture anomalies for the representative grids from (a) NE, (b) HR, (c) CNE, (d) PR, (e) WC and (f) NW for the year 1993. The anomalies are calculated as the difference between the value of the state variable and the climatological mean divided by the standard deviation for that pentad. Daily soil moisture was converted to pentad-scale using 5-day moving average, resulting in 73 pentads in a year.

3.3 Flash drought mechanisms

At the six selected locations, we identified flash drought periods based on the model-simulated soil moisture percentiles. We analyse the changes in state variables caused by external forcings and the system response driven by the state variables. We find that all flash droughts occur during periods of deficient rainfall and the drying is predominantly driven by net shortwave radiation. However, the flash droughts differ in terms of contribution of winds towards drying, based on which we classify the flash drought mechanisms into three types: (a) Category 1: flash droughts with wind-driven intensification due to land-atmospheric feedback (b) Category 2: flash droughts with minimal contribution of winds towards drying and (c) Category 3: flash droughts with wind-driven intensification due to advected heat. We describe the three mechanisms using three representative flash drought events.

3.3.1 Flash droughts with wind-driven intensification due to land-atmospheric feedback

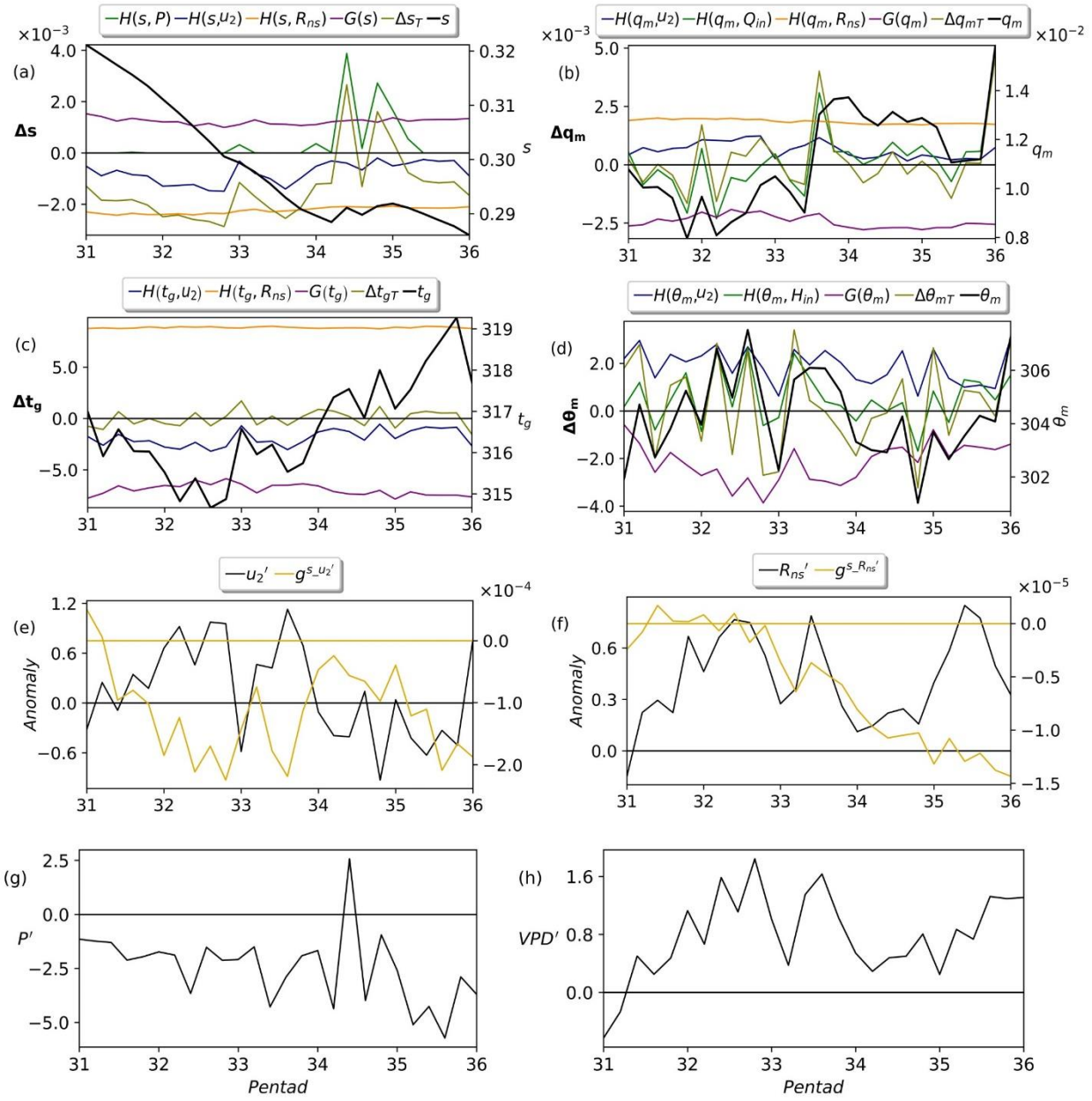

Figure 3: Example of a Category 1 flash drought which occurred in June 2012 in the NW region. Figures (a-d) show the time series of the state variables (black) and daily changes in the state variables (olive). The daily changes in state variables are decomposed into those caused by system response G (purple) and forcings H. The blue and orange lines represent the individual contributions of winds and shortwave radiation towards changes in the state variable. Green line represents precipitation contribution to change in soil moisture in (a) and contribution of external advection to changes in respective state variables in (b) and (d). Anomalies of (e) wind velocity, (f) net shortwave radiation, (g) precipitation and (h) VPD are shown by black solid lines. The anomalies are calculated as the difference between values of the state variable and the climatological mean for that pentad. The yellow lines in (e-f) represent anomalies in sensitivities of soil moisture with respect to wind and shortwave radiation and are plotted on secondary Y-axis. The notation $H(X, F)$ represents changes in state variable (X) induced by forcing (F) individually. $G(X)$ represents systems response to changes induced in X.

Figure 3 illustrates the evolution of forcings, state variables and sensitivity of changes in state variables to forcings during a flash drought in the NW region, which occurred in June 2012. Figure 3a shows the soil moisture during the flash drought period in black and the daily changes in olive. The daily changes in soil moisture are decomposed into changes caused by state variables (shown in purple) and those caused by each forcings, with the changes caused by precipitation, wind and shortwave radiation shown in green, blue, and orange respectively. Similarly, Figures 3b-d show the daily changes and their decomposition into forcing- and state-driven changes for humidity, ground temperature and air temperature respectively. Figures 3e-h show the anomalies of wind velocity, shortwave radiation, precipitation and VPD respectively during the flash drought.

During the flash drought event shown in Figure 3, the soil moisture percentiles fell from above 40th to below 20th percentile between pentads 33 and 36 (Figure S4). Figure 3 shows that external forcings contribute to a negative change of soil moisture, whereas the system-driven response negates this effect through higher upward longwave radiation RL_{gu}, which reduces the net energy available for evaporation (Equation 12a). However, since the changes in soil moisture caused by external forcings are larger, soil moisture rapidly declines during this period. The changes in soil moisture are controlled by three external forcings: 1) precipitation (P), 2) net shortwave radiation (R_{ns}) and 3) wind speed (u_2). The flash drought occurs in a period of deficient rainfall (Figure 3g). Figure 3a shows that net shortwave radiation contributes most significantly to soil moisture depletion (orange line) followed by wind speed (blue line), which is due to large positive anomalies of net shortwave radiation and persistent evaporation (Figure 3f).

While the contribution of R_{ns} to soil moisture depletion remains almost constant throughout the flash drought, wind contributes to rapid intensification of drying of soil between pentads 32 and 34 (Figure 3a). This period of rapid drying is driven by an increase in sensitivity of wind velocity to changes in soil moisture $(g^{s\_u_2})$ and high anomaly in wind speed at same time (Figure 3e). It is important to note that $g^{s\_u_2}$ is negative as higher wind velocity leads to depletion of soil moisture through evapotranspiration (equation 16). Hence, negative anomalies of $g^{s\_u_2}$ denote increased sensitivity of soil moisture with respect to wind. The sensitivity of winds to reduction in soil moisture is controlled by three factors: 1) β, 2) $\frac{b_2}{\theta_m}$ and 3) VPD. Out of these three factors, VPD had the largest positive anomalies during this period and hence contributed to negative anomalies in in $g^{s\_u_2}$ (Figure 3h), while the contributions of the other two components were not significant (Figure S7 in supporting information).

VPD is the difference between the saturation vapour pressure, which depends on the air temperature, and the actual vapour pressure which depends on the specific humidity of air. Thus, the increase in VPD during the flash droughts could be caused by increased air temperature, decreased specific humidity or a combination of both. The changes and drivers of specific humidity and air temperature are shown in Figure 3b and Figure 3d respectively. It is evident from Figure 3b that the specific humidity was lowered predominantly due to advection of dry winds (green line in Figure 3b), whereas air temperature increased through winds due to sensible heating (Equation

22) as shown by the blue line in Figure 3d. The high sensible heating can be attributed to increased land surface temperature driven by net shortwave radiation and lack of evaporative cooling due to low soil moisture (Figure 3c).

In summary, the soil moisture depletion of category 1 flash droughts is predominantly driven by shortwave radiation during a period of low precipitation. Due to low evaporative cooling, the shortwave radiation heats up the land, leading to increased sensible heating which in turn contributes to higher air temperature. The high air temperature combined with low humidity due to advection of dry wind from upwind areas lead to increased VPD. The increased VPD increases the propensity of winds to evaporate water from soil, which further depletes soil moisture, and the ground temperature increases. This mechanism is a classic example of land atmosphere feedback accelerating the rate of drying of soil.

3.3.2 Flash droughts with minimal contribution of wind towards drying

Figure 4 shows the evolution of state variables, forcings, their corresponding sensitivities and individual forcing contributions during a flash drought event which occurred in March-April 1993 in the SP region. The representation of all variables is similar to that of Figure 3. Soil moisture percentiles fell from above 40th to below 20th percentile between pentads 17 and 20 (Figure S5). Figure 4a shows that the drying of soil is driven by shortwave radiation (orange line), whereas the contribution of wind is negligible (blue line). Below normal precipitation accompanied with persistent evapotranspiration from the soil due to positive shortwave radiation anomalies (Figure 4f) leads to the drying of soil. We find that flash droughts of category 2 frequently occur in humid regions where the initial soil moisture levels are high. The negligible effect of winds on drying is due to smaller values of $g^{s\_u_2}$ (Figure 4e). Shortwave radiation leads to increase in ground temperature (orange line in Figure 4c) and a subsequent increase in air temperature through sensible heating (blue line in Figure 4d), but it does not translate to increase in VPD (Figure 4h) as the magnitude of air temperature is much lower as compared to category 1 flash droughts. Furthermore, the specific humidity of air also does not decrease during the flash drought due to moisture supply from shortwave radiation driven evaporation (Figure 4b and Figure S5). Out of the other two components of term $g^{s\_u_2}$, β was always negatively anomaly and $\frac{b_2}{\theta_m}$ also do not have significantly high anomalies to have strong influence (Figure S8). As a result, there is no significant rise in $g^{s\_u_2}$, due to which winds do not intensify the rates of drying.

To summarize, in category 2 flash droughts, which are often seen in humid regions, the drying of soils is driven by shortwave radiation and winds do not have any significant influence. The increase in VPD during the flash droughts is restricted by the low magnitude of atmospheric temperature due to high latent heat flux and high specific humidity due to high evaporation rates, thereby preventing the intensification of flash droughts by winds.

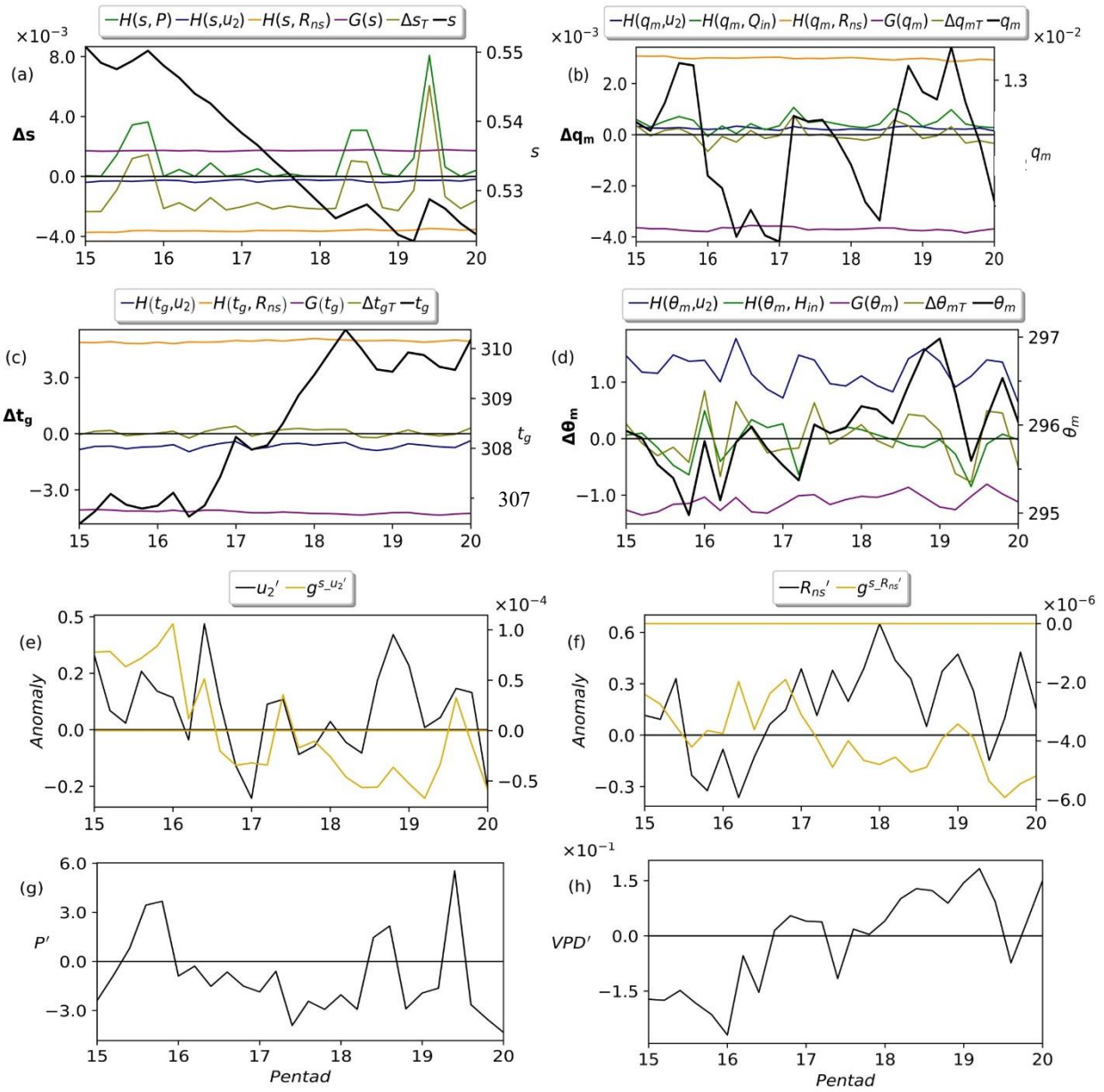

Figure 4 Example of a Category 2 flash drought which occurred in March-April 1993 in the SP region. Figures (a-d) show the time series of the state variables (black) and daily changes in the state variables (olive). The daily changes in state variables are decomposed into those caused by system response G (purple) and forcings H. The blue and orange lines represent the individual contributions of winds and shortwave radiation towards changes in the state variable. Green line represents precipitation contribution to change in soil moisture in (a) and contribution of external advection to changes in respective state variables in (b) and (d). Anomalies of (e) wind velocity, (f) net shortwave radiation, (g) precipitation and (h) VPD are shown by black solid lines. The anomalies are calculated as the difference between values of the state variable and the climatological mean for that pentad. The yellow lines in (e-f) represent anomalies in sensitivities of soil moisture with respect to wind and shortwave radiation and are plotted on secondary Y-axis. The notation $H(X,F)$ represents changes in state variable (X) induced by forcing (F) individually. $G(X)$ represents systems response to changes induced in X.

3.3.3 Flash droughts with wind-driven intensification due to advected heat

We also identified some flash droughts which though lesser in frequency, have a different developing mechanism than Category 1 and Category 2 flash droughts. While the rate of drying of soil is intensified by winds, what distinguishes them from Category 1 flash droughts is that the advection of hot air from upwind areas is a more important contributor to increase in VPD than sensible heating. Thus, the flash droughts of this category are influenced by climatic conditions in the upwind areas. Figure 5 illustrates a flash drought of this kind which occurred in the NW region during January-February 1993. The representation of all variables is similar to that of Figure 3 and Figure 4. Soil moisture percentiles fell from above 40th to below 20th percentile between pentads 3 and 8 (Figure S6). From Figure 5a it can be seen that there was an intensification of the drying of soil in the 7th and 8th pentad. As shown in Figure 5a, the contribution of winds (blue line) towards soil moisture depletion is comparable to that of shortwave radiation (orange line) and the winds played an important role in the intensification of the flash drought in the 7th and 8th pentads. This is due to high anomaly in sensitivity of soil moisture to winds in the 8th pentad (negative $g^{s\_u_2}$ in Figure 5e). The increased sensitivity of winds is caused by a sharp spike in VPD (Figure 5j and Figure S9), which can be attributed to decreased specific humidity (Figures 5b and S6) and increased air temperature (Figures 5d and Figure S6). The other two components of $g^{s\_u_2}$: β and $\frac{b_2}{\theta_m}$ had negative anomalies (Figure S9) and hence did not contribute to increase in $g^{s\_u_2}$. The green lines in Figures 5b and 5d show that advection was the major contributor to increase in air temperature and decrease in specific humidity during the intensification period, which led to the sharp increase in VPD.

Thus, Category 3 flash droughts apart from shortwave radiation, are also influenced by winds. This influence comes from increased sensitivity to winds which is a result of increased VPD. The increase in VPD is a result of advection of dry and heated air from the upwind areas which directly increases atmospheric temperature and not the ground temperature. Land atmosphere interaction is only one way in these flash droughts and coupling is absent. We observe that in many cases of Category 3 flash droughts, both sensitivity of winds and magnitude of winds are high at the same time.

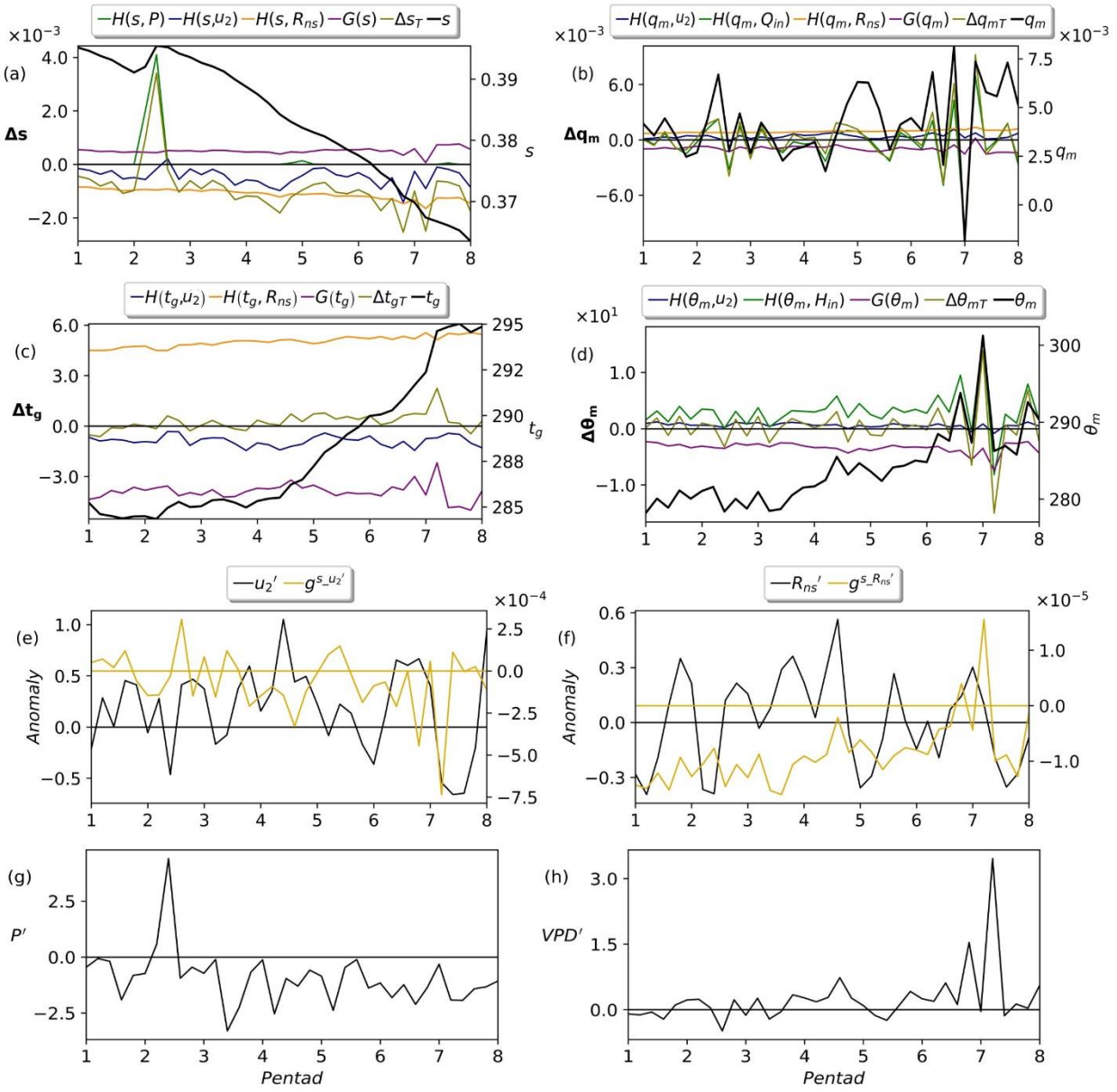

Figure 5 Example of a Category 3 flash drought which occurred in January-February 1993 in the NW region. Figures (a-d) show the time series of the state variables (black) and daily changes in the state variables (olive). The daily changes in state variables are decomposed into those caused by system response G (purple) and forcings H. The blue and orange lines represent the individual contributions of winds and shortwave radiation towards changes in the state variable. Green line represents precipitation contribution to change in soil moisture in (a) and contribution of external advection to changes in respective state variables in (b) and (d). Anomalies of (e) wind velocity, (f) net shortwave radiation, (g) precipitation and (h) VPD are shown by black solid lines. The anomalies are calculated as the difference between values of the state variable and the climatological mean for that pentad. The yellow lines in (e-f) represent anomalies in sensitivities of soil moisture with respect to wind and shortwave radiation and are plotted on secondary Y-axis. *The notation $H(X,F)$ represents changes in state variable (X) induced by forcing (F) individually. $G(X)$ represents systems response to changes induced in X.*

4 Discussion

4.1 Seasonal variation of flash drought mechanisms

The Indian Meteorological Department (IMD) classifies Indian weather system into four seasons as, S1 Winter (JF), S2 Pre-monsoon (MAM), S3 Monsoon (JJAS) and S4 Post-monsoon (OND) (IMD annual report, 2022). Since the forcings and state variables have seasonal variations, the mechanisms of flash droughts can also vary across seasons. Having discussed the major flash drought mechanisms, we calculate the frequency of occurrence of each kind of flash drought in different seasons, across selected regions, which is shown in Figure 6. As evident in the figure, flash droughts occur most frequently in the monsoon season. Active and break spells are a common feature of the Indian monsoon (Rajeevan et al., 2010). We find that most of the flash droughts in the monsoon season occur during the monsoon breaks. Furthermore, we find that the majority of flash droughts in the monsoon season are Category 2 flash droughts, which are driven by persistent evapotranspiration due to shortwave radiation. The high frequency of Category 2 flash droughts in the monsoon season can be attributed to high shortwave radiation during June-August and high soil moisture from the active spells of monsoon. Category 2 flash droughts also occur in the pre-monsoon and post-monsoon season, but these are mostly observed in humid regions of NE and SP, which receive significant rainfall in these seasons.

We find that category 1 and category 3 flash droughts occur in the pre-monsoon and monsoon period due to high wind speeds during this period. Since shortwave radiation is the major driver of all identified flash droughts, the frequency of flash droughts is the lowest in the post-monsoon and winter seasons.

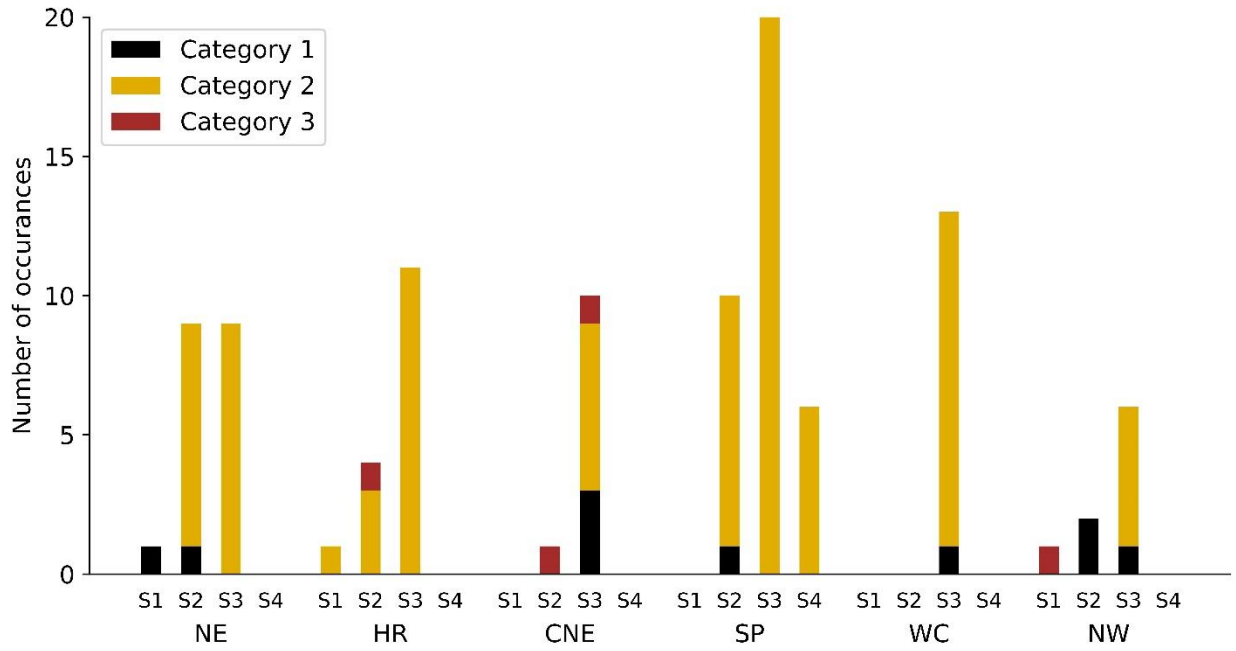

Figure6: Frequency of Category 1 (black), Category 2 (yellow) and Category 3 (brown) flash droughts in different seasons and regions of India. The Indian meteorological department (IMD) categorizes Indian weather system into four categories namely winter (Jan-Feb), pre-monsoon (Mar-May), monsoon (June-Sep), post-monsoon (Oct-Dec) which are represented in this figure with bars S1, S2, S3 and S4 respectively.

4.2 Development time of flash droughts

Figure 7 shows the comparison of drought development times of the three types of flash droughts. We calculate the development times as the duration in which soil moisture falls from above 40th percentile to below 20th percentile. The figure shows that Category 3 flash droughts which are observed in only three regions (Figure 6), evolve the slowest. Most of these flash droughts are observed in the CNE region (Figure 6). These kinds of flash droughts, which occur in the pre-monsoon or monsoon season of the year are driven by hot and dry westerly winds known as 'loo' (Walker et al., 2024). Category 1 flash drought develop faster as compared to Category 3 flash droughts and Category 2 flash droughts on average due to the role of land-atmospheric interaction in the intensification of Category 1 flash droughts. Category 2 flash droughts occur most frequently among the three categories and in all the six regions. Their frequency is particularly higher in the Northeast and South Peninsular region which have humid climates and hence high soil moisture levels (Figure 6). We also found that the flash drought development period is shorter in these two regions compared to other regions due to higher evaporation efficiency at higher soil moisture levels (Figure S10 in the supporting information). On the other hand, the Himalayan region has the highest drought development period due to smaller evaporation efficiency (Figure S10).

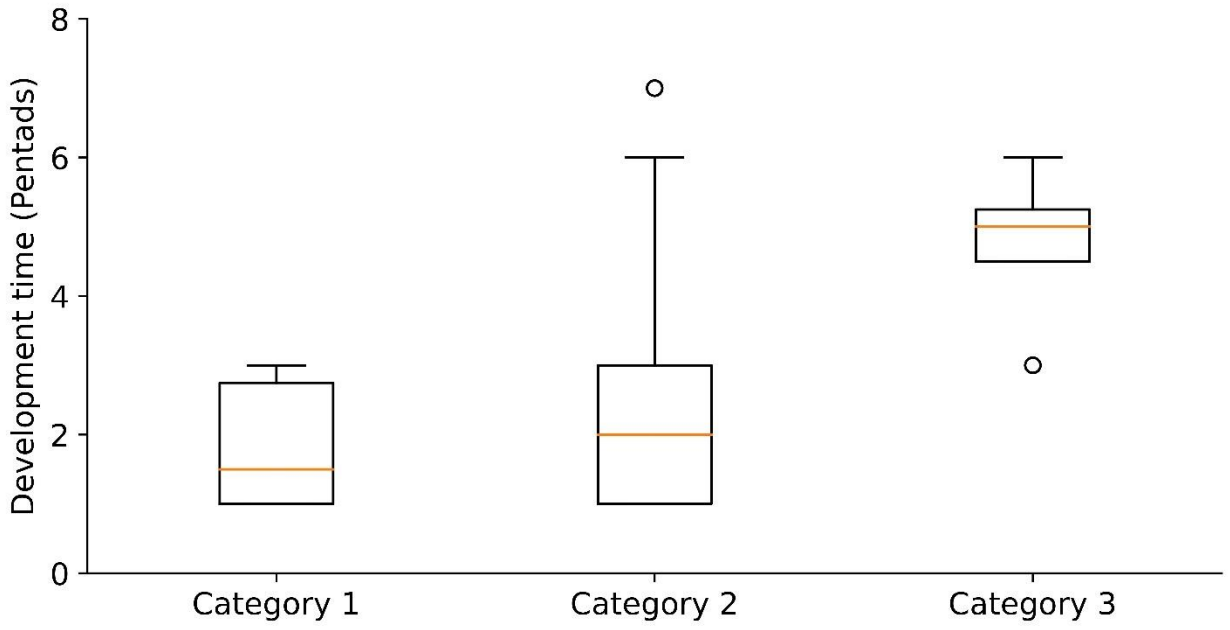

Figure 7: Box plots of drought development time of Category 1, Category 2 and Category 3 flash droughts averaged over all seasons and regions of India. The drought development time is the period in pentads in which soil moisture falls from above 40th percentile to below 20th percentile.

4.3 Influence of vapor pressure deficit (VPD) on development of flash droughts

Many previous studies have identified VPD as a strong driver of flash droughts (Gamelin et al., 2022; Mahto & Mishra, 2023). According to these studies, increased VPD increases ET from the soil which results in development of flash droughts. These studies suggest that due to land atmosphere interaction, the atmosphere gets heated which further extracts moisture from the soil (Category 1 flash droughts). However, most of these have used statistical techniques such as anomaly calculations or using coupling diagnostics for arriving at these conclusions (Qing et al., 2022; Y. Wang & Yuan, 2022). However, in this study we use an analytical approach to quantify the influence of each flash drought driver on development of flash drought. We find that in India, persistent evapotranspiration driven by shortwave radiation along with below normal precipitation leads to rapid extraction of moisture from the soil in majority of flash droughts. We find that the instances of flash droughts with wind-driven intensification due to land atmosphere interaction (Category 1) are fewer than the flash droughts driven by shortwave radiation (Category 2). We find that Category 2 flash droughts are also associated with an increase in VPD, but it does not have a significant impact on the rate of drying of soils. We find that out of the total identified flash droughts, VPD increases in 81.6 % of the flash droughts but it contributes to rapid drying of soils in only 14.2 % of the flash droughts. Furthermore, we find that land-atmospheric feedback contributes to intensification of only 10.2% of the flash droughts. We find that VPD intensifies the rate of drying of soil when the wind velocity and the magnitude of VPD are high at the same time, which does not happen frequently.

Our study shows that due to the complex and non-linear interactions between land and atmospheric processes, the use of linear statistical approaches can lead to misleading conclusions. While flash droughts are associated with positive VPD anomalies, which can result in significant correlation coefficients or diagnostic metrics, VPD may not be the actual driver of flash drought, as we show in case of Indian flash droughts. This highlights the importance of physically based frameworks for studies on land-atmospheric interactions.

4.4 Limitations

In this study, we developed an analytical approach to understand flash drought mechanisms based on the water and energy balance equations of a simplified land-atmospheric model. The model has a static representation of the atmosphere due to which the effects of changes in boundary layer height are not modelled, which can significantly affect the energy balance of the atmosphere during dry events. Increase in boundary layer height and the corresponding heat entrainment have been shown to be key contributors to temperature rise during heatwaves (Miralles et al., 2014). The model also lacks any representation of the vegetation dynamics. Plant species can have varied response to flash droughts, depending on their hydraulic traits (Brodribb et al., 2020), which can influence land-atmospheric interactions and the intensification of flash droughts (Anderegg et al., 2019). While more accurate and sophisticated land-atmosphere models like Variable Infiltration Capacity (VIC) model (Liang et al., 1994), Community Land Model (CLM) (Bonan et al., 2002) and Community Climate System Model (CCSM) (Dickinson et al., 2006) are available, the interpretation of the physical mechanisms of flash droughts becomes challenging in these models due to the complex multivariate equations and multi-layered model structure. That is why, in this study we adopt a diagnostic approach and utilise the analytical tractability of a simple land-atmospheric model to understand flash drought mechanisms. Although the simplified representation of processes may lower the accuracy of the model, the objective of this study it to capture the major physical mechanisms that contribute to rapid drying during flash droughts. To that end, results in Figure 2 show that our model can capture most of the flash drought events in all precipitation regions across India.

5.Conclusions

We develop an analytical framework to quantify the contributions of external forcings and system-driven changes towards changes in the state variables during flash droughts. The framework is based on the energy and water balance equations of a lumped land-atmospheric model. We apply the framework for analysing the physical mechanisms of flash droughts in India. We identified three major flash drought mechanisms in India. In Category 1 flash droughts, the drying of soil is driven by net shortwave radiation and intensified by land-atmospheric feedback. In these flash droughts, increased VPD due to sensible heating combined with high wind velocity accelerates the rate of drying of soil. In Category 2 flash droughts, the drying of soil is driven by high shortwave

radiation with negligible role of wind. In category 3 flash droughts, the advection of hot and dry winds from upwind areas increases the atmospheric temperature and hence VPD which further accelerates the drying of soil. Most flash droughts in India belong to Category 2 and occur during the monsoon or pre-monsoon season, with the highest frequency in the moisture rich NE and SP regions. We find that the drought development time of Category 3 flash drought is highest while Category 1 flash droughts intensify most rapidly due to land atmospheric feedback. We show that while increased VPD is a frequently recurring feature of flash droughts, it is not necessarily a significant contributor to flash drought intensification. Hence, approaches based on correlation of VPD to soil moisture drop and flash drought occurrences might provide misleading understanding of flash drought mechanisms.

Data availability statement:

The data used in this study is available at open access from Copernicus climate data store (CDS). It can be accessed using below links.

1. https://cds.climate.copernicus.eu/cdsapp#!/dataset/reanalysis-era5-single-levels?tab=overview
2. https://cds.climate.copernicus.eu/cdsapp#!/dataset/reanalysis-era5-pressure-levels?tab=form

Acknowledgement:

We are grateful for the research scholar fellowship provided by the Ministry of Education, Government of India. We acknowledge and thank them for their support throughout the research work.

Appendix

The constant used in this study are below

Table A1: Constants used in this study

1.	Dry air specific heat at constant pressure (c_p)	1005 J/Kg/K
2.	Stefen Boltzmann constant (σ)	$4.903 \times 10^{-9}\ MJm^{-2}day^{-1}K^{-4}$
3.	Latent heat of vaporization of water (λ)	24.5×10^{5} JKg^{-1}
4.	Density of air (ρ)	1.225 Kg m^{-3}
5.	Density of liquid water (ρ_w)	997 Kg m^{-3}
6.	Gas constant for dry air (r_d)	$287.053\ Jkg^{-1}K - 1$

Following parameters were referred from (Brubaker & Entekhabi, 1995) :

Table A2: Parameters taken from original BE95 model of (Brubaker & Entekhabi, 1995)

1.	Coefficient of sensible heat (c_1)	0.001
2.	Exponent of evaporation efficiency (c)	1
3.	Exponent of runoff ratio (r)	2
4.	Coefficient of runoff ratio (η)	1
5.	Mixed layer emissivity (ϵ_m) (after integration of BE95 expression)	0.56

References

Ahmad, S. K., Kumar, S. V., Lahmers, T. M., Wang, S., Liu, P. W., Wrzesien, M. L., Bindlish, R., Getirana, A., Locke, K. A., Holmes, T. R., & Otkin, J. A. (2022). Flash Drought Onset and Development Mechanisms Captured With Soil Moisture and Vegetation Data Assimilation. *Water Resources Research*, *58*(12). https://doi.org/10.1029/2022WR032894

Allen, R. G., Pereira, L. S., & Raes, D. (1998). *Crop Evapotranspiration (guidelines for computing crop water requirements)*.

Anderegg, W. R. L., Trugman, A. T., Bowling, D. R., Salvucci, G., & Tuttle, S. E. (2019). Plant functional traits and climate influence drought intensification and land–atmosphere feedbacks. *Proceedings of the National Academy of Sciences of the United States of America*, *116*(28), 14071–14076. https://doi.org/10.1073/pnas.1904747116

Anderson, M. C., Norman, J. M., Mecikalski, J. R., Otkin, J. A., & Kustas, W. P. (2007). A climatological study of evapotranspiration and moisture stress across the continental United States based on thermal remote sensing: 2. Surface moisture climatology. *Journal of Geophysical Research Atmospheres*, *112*(11). https://doi.org/10.1029/2006JD007507

Basara, J. B., Christian, J. I., Wakefield, R. A., Otkin, J. A., Hunt, E. H., & Brown, D. P. (2019). The evolution, propagation, and spread of flash drought in the Central United States during 2012. *Environmental Research Letters*, *14*(8). https://doi.org/10.1088/1748-9326/ab2cc0

Bonan, G. B., Levis, S., Kergoat, L., & Oleson, K. W. (2002). Landscapes as patches of plant functional types: An integrating concept for climate and ecosystem models. *Global Biogeochemical Cycles*, *16*(2), 5-1-5–23. https://doi.org/10.1029/2000gb001360

Brodribb, T. J., Powers, J., Cochard, H., & Choat, B. (2020). Hanging by a thread? Forests and drought. *Science*, *368*(6488), 261–266. https://doi.org/10.1126/science.aat7631

Brubaker, K. L., & Entekhabi, D. (1995). An Analytic Approach to Modeling Land-Atmosphere Interaction: 1. Construct and Equilibrium Behavior. *Water Resources Research*, *31*(3), 619–632. https://doi.org/10.1029/94WR01772

Chandra, D. G., & Malaya, D. B. (2011). Role of e-Agriculture in Rural Development in Indian Context. *2011 International Conference on Emerging Trends in Networks and Computer Communications (ETNCC)*, 320–323. https://doi.org/10.1109/ETNCC.2011.6255913

Chen, L. G., Gottschalck, J., Hartman, A., Miskus, D., Tinker, R., & Artusa, A. (2019). Flash drought characteristics based on U.S. drought monitor. *Atmosphere*, *10*(9). https://doi.org/10.3390/atmos10090498

Christian, J. I., Basara, J. B., Hunt, E. D., Otkin, J. A., Furtado, J. C., Mishra, V., Xiao, X., & Randall, R. M. (2021). Global distribution, trends, and drivers of flash drought occurrence. *Nature Communications*, *12*(1). https://doi.org/10.1038/s41467-021-26692-z

Christian, J. I., Martin, E. R., Basara, J. B., Furtado, J. C., Otkin, J. A., Lowman, L. E. L., Hunt, E. D., Mishra, V., & Xiao, X. (2023). Global projections of flash drought show increased risk in a warming climate. *Communications Earth and Environment*, *4*(1). https://doi.org/10.1038/s43247-023-00826-1

Das, J., Das, S., & Umamahesh, N. V. (2023). Surface latent and sensible heat trigger flash drought events in India. *Hydrological Processes*, *37*(11). https://doi.org/10.1002/hyp.15037

Dhawan, V. (2017). *Water and Agriculture in India*. http://www.yourarticlelibrary.com/essay/essay-on-water-scarcity-in-india-1113-words/20871/

Dickinson, R. E., Oleson, K. W., Bonan, G., Hoffman, F., Thornton, P., Vertenstein, M., Yang, Z.-L., & Zeng, X. (2006). *The Community Land Model and Its Climate Statistics as a Component of the Community Climate System Model*.

Entekhabi, D., & Brubaker, K. L. (1995). An analytic approach to modeling land-atmosphere interaction 2. Stochastic formulation. In *WATER RESOURCES RESEARCH* (Vol. 31, Issue 3).

Ford, T. W., & Labosier, C. F. (2017). Meteorological conditions associated with the onset of flash drought in the Eastern United States. *Agricultural and Forest Meteorology*, *247*, 414–423. https://doi.org/10.1016/j.agrformet.2017.08.031

Gamelin, B. L., Feinstein, J., Wang, J., Bessac, J., Yan, E., & Kotamarthi, V. R. (2022). Projected U.S. drought extremes through the twenty-first century with vapor pressure deficit. *Scientific Reports*, *12*(1). https://doi.org/10.1038/s41598-022-12516-7

Gong, Z., Zhu, J., Li, T., Huang, D., Chen, X., & Zhang, Q. (2022). The features of regional flash droughts in four typical areas over China and the possible mechanisms. *Science of the Total Environment*, *827*. https://doi.org/10.1016/j.scitotenv.2022.154217

Han, J., Zhang, J., Yang, S., & Seka, A. M. (2023). Improved Understanding of Flash Drought from a Comparative Analysis of Drought with Different Intensification Rates. *Remote Sensing*, *15*(8). https://doi.org/10.3390/rs15082049

Hersbach, H., Bell, B., Berrisford, P., Hirahara, S., Horányi, A., Muñoz-Sabater, J., Nicolas, J., Peubey, C., Radu, R., Schepers, D., Simmons, A., Soci, C., Abdalla, S., Abellan, X., Balsamo, G., Bechtold, P., Biavati, G., Bidlot, J., Bonavita, M., … Thépaut, J. N. (2020). The ERA5 global reanalysis. *Quarterly Journal of the Royal Meteorological Society*, *146*(730), 1999–2049. https://doi.org/10.1002/qj.3803

Hobbins, M. T. (2016). The variability of ASCE Standardized reference evapotranspiration: A rigorous, CONUS-wide decomposition and attribution. *Transactions of the ASABE*, *59*(2), 561–576. https://doi.org/10.13031/trans.59.10975

Hobbins, M. T., Wood, A., McEvoy, D. J., Huntington, J. L., Morton, C., Anderson, M., & Hain, C. (2016a). The evaporative demand drought index. Part I: Linking drought evolution to variations in evaporative demand. *Journal of Hydrometeorology*, *17*(6), 1745–1761. https://doi.org/10.1175/JHM-D-15-0121.1

Hobbins, M. T., Wood, A., McEvoy, D. J., Huntington, J. L., Morton, C., Anderson, M., & Hain, C. (2016b). The evaporative demand drought index. Part I: Linking drought evolution to variations in evaporative demand. *Journal of Hydrometeorology*, *17*(6), 1745–1761. https://doi.org/10.1175/JHM-D-15-0121.1

Hoffmann, D., Gallant, A. J. E., & Hobbins, M. (n.d.). *Flash Drought in CMIP5 Models*. https://doi.org/10.1175/JHM-D-20

Huang, P. M., Li, Y., & Sumner, M. E. (Eds.). (2011). *Handbook of Soil Sciences*. CRC Press. https://doi.org/10.1201/b11267

Hunt, E. D., Svoboda, M., Wardlow, B., Hubbard, K., Hayes, M., & Arkebauer, T. (2014). Monitoring the effects of rapid onset of drought on non-irrigated maize with agronomic data and climate-based drought indices. *Agricultural and Forest Meteorology*, *191*, 1–11. https://doi.org/10.1016/j.agrformet.2014.02.001

IMD annual report. (2022). *वा◆षर ृ ◆ितवे दन ANNUAL REPORT 2022 INDIA METEOROLOGICAL DEPARTMENT (MINISTRY OF EARTH SCIENCES)*. https://mausamjournal.imd.gov.in/

Joshi, P. A. (2015). Challenges of agriculture economy of India. In *The Business & Management Review* (Vol. 5).

Koster, R. D., Schubert, S. D., Wang, H., Mahanama, S. P., & Deangelis, A. M. (2019). Flash drought as captured by reanalysis data: Disentangling the contributions of precipitation deficit and excess evapotranspiration. *Journal of Hydrometeorology*, *20*(6), 1241–1258. https://doi.org/10.1175/JHM-D-18-0242.1

Liang, X., Lettenmaier, D. P., Wood, E. F., & Burges, S. J. (1994). A simple hydrologically based model of land surface water and energy fluxes for general circulation models. In *JOURNAL OF GEOPHYSICAL RESEARCH* (Vol. 99, Issue D7).

Lisonbee, J., Woloszyn, M., & Skumanich, M. (2021). Making sense of flash drought: definitions, indicators, and where we go from here. *Journal of Applied and Service Climatology*, *2021*(1), 1–19. https://doi.org/10.46275/joasc.2021.02.001

Liu, Z., Zhou, W., & Yuan, Y. (2023). 3D DBSCAN detection and parameter sensitivity of the 2022 Yangtze river summertime heatwave and drought. *Atmospheric and Oceanic Science Letters*, *16*(4). https://doi.org/10.1016/j.aosl.2022.100324

Lorenz, D. J., Otkin, J. A., Svoboda, M., Hain, C. R., Anderson, M. C., & Zhong, Y. (2017). Predicting U.S. drought monitor states using precipitation, soil moisture, and evapotranspiration anomalies. Part I: Development of a nondiscrete USDM index. *Journal of Hydrometeorology*, *18*(7), 1943–1962. https://doi.org/10.1175/JHM-D-16-0066.1

Mahto, S. S., & Mishra, V. (2020a). Dominance of summer monsoon flash droughts in India. *Environmental Research Letters*, *15*(10). https://doi.org/10.1088/1748-9326/abaf1d

Mahto, S. S., & Mishra, V. (2020b). Dominance of summer monsoon flash droughts in India. *Environmental Research Letters*, *15*(10). https://doi.org/10.1088/1748-9326/abaf1d

Mahto, S. S., & Mishra, V. (2023). Flash drought intensification due to enhanced land-atmospheric coupling in India. *Journal of Climate*, 1–31. https://doi.org/10.1175/jcli-d-22-0477.1

Miralles, D. G., Gentine, P., Seneviratne, S. I., & Teuling, A. J. (2019). Land–atmospheric feedbacks during droughts and heatwaves: state of the science and current challenges. *Annals of the New York Academy of Sciences*, *1436*(1), 19–35. https://doi.org/10.1111/nyas.13912

Miralles, D. G., Teuling, A. J., Van Heerwaarden, C. C., & De Arellano, J. V. G. (2014). Mega-heatwave temperatures due to combined soil desiccation and atmospheric heat accumulation. *Nature Geoscience*, *7*(5), 345–349. https://doi.org/10.1038/ngeo2141

Mishra, V., Aadhar, S., & Mahto, S. S. (2021a). Anthropogenic warming and intraseasonal summer monsoon variability amplify the risk of future flash droughts in India. *Npj Climate and Atmospheric Science*, *4*(1). https://doi.org/10.1038/s41612-020-00158-3

Mishra, V., Aadhar, S., & Mahto, S. S. (2021b). Anthropogenic warming and intraseasonal summer monsoon variability amplify the risk of future flash droughts in India. *Npj Climate and Atmospheric Science*, *4*(1). https://doi.org/10.1038/s41612-020-00158-3

Mo, K. C., & Lettenmaier, D. P. (2015). Heat wave flash droughts in decline. *Geophysical Research Letters*, *42*(8), 2823–2829. https://doi.org/10.1002/2015GL064018

Mo, K. C., & Lettenmaier, D. P. (2016). Precipitation deficit flash droughts over the United States. *Journal of Hydrometeorology*, *17*(4), 1169–1184. https://doi.org/10.1175/JHM-D-15-0158.1

Noguera, I., Domínguez-Castro, F., & Vicente-Serrano, S. M. (2021). Flash drought response to precipitation and atmospheric evaporative demand in spain. *Atmosphere*, *12*(2), 1–22. https://doi.org/10.3390/atmos12020165

Orlowsky, B., & Seneviratne, S. I. (2010). Statistical analyses of land-atmosphere feedbacks and their possible pitfalls. *Journal of Climate*, *23*(14), 3918–3932. https://doi.org/10.1175/2010JCLI3366.1

Osman, M., Zaitchik, B. F., Badr, H. S., Otkin, J., Zhong, Y., Lorenz, D., Anderson, M., Keenan, T. F., Miller, D. L., Hain, C., & Holmes, T. (n.d.). *Diagnostic Classification of Flash Drought Events Reveals Distinct Classes of Forcings and Impacts*. https://doi.org/10.1175/10.1175/JHM

Otkin, J. A., Anderson, M. C., Hain, C., Mladenova, I. E., Basara, J. B., & Svoboda, M. (2013). Examining rapid onset drought development using the thermal infrared-based evaporative stress index. *Journal of Hydrometeorology*, *14*(4), 1057–1074. https://doi.org/10.1175/JHM-D-12-0144.1

Otkin, J. A., Haigh, T., Mucia, A., Anderson, M. C., & Hain, C. (2018). Comparison of agricultural stakeholder survey results and drought monitoring datasets during the 2016 u.S. northern plains flash drought. *Weather, Climate, and Society*, *10*(4), 867–883. https://doi.org/10.1175/WCAS-D-18-0051.1

Otkin, J. A., Svoboda, M., Hunt, E. D., Ford, T. W., Anderson, M. C., Hain, C., & Basara, J. B. (2018). Flash droughts: A review and assessment of the challenges imposed by rapid-

onset droughts in the United States. In *Bulletin of the American Meteorological Society* (Vol. 99, Issue 5, pp. 911–919). American Meteorological Society. https://doi.org/10.1175/BAMS-D-17-0149.1

Otkin, J. A., Zhong, Y., Hunt, E. D., Christian, J. I., Basara, J. B., Nguyen, H., Wheeler, M. C., Ford, T. W., Hoell, A., Svoboda, M., & Anderson, M. C. (2021). Development of a flash drought intensity index. *Atmosphere*, *12*(6). https://doi.org/10.3390/atmos12060741

Parker, T., Gallant, A., Hobbins, M., & Hoffmann, D. (2021). Flash drought in Australia and its relationship to evaporative demand. *Environmental Research Letters*, *16*(6). https://doi.org/10.1088/1748-9326/abfe2c

Pendergrass, A. G., Meehl, G. A., Pulwarty, R., Hobbins, M., Hoell, A., AghaKouchak, A., Bonfils, C. J. W., Gallant, A. J. E., Hoerling, M., Hoffmann, D., Kaatz, L., Lehner, F., Llewellyn, D., Mote, P., Neale, R. B., Overpeck, J. T., Sheffield, A., Stahl, K., Svoboda, M., … Woodhouse, C. A. (2020a). Flash droughts present a new challenge for subseasonal-to-seasonal prediction. *Nature Climate Change*, *10*(3), 191–199. https://doi.org/10.1038/s41558-020-0709-0

Pendergrass, A. G., Meehl, G. A., Pulwarty, R., Hobbins, M., Hoell, A., AghaKouchak, A., Bonfils, C. J. W., Gallant, A. J. E., Hoerling, M., Hoffmann, D., Kaatz, L., Lehner, F., Llewellyn, D., Mote, P., Neale, R. B., Overpeck, J. T., Sheffield, A., Stahl, K., Svoboda, M., … Woodhouse, C. A. (2020b). Flash droughts present a new challenge for subseasonal-to-seasonal prediction. In *Nature Climate Change* (Vol. 10, Issue 3, pp. 191–199). Nature Research. https://doi.org/10.1038/s41558-020-0709-0

Qing, Y., Wang, S., Ancell, B. C., & Yang, Z. L. (2022). Accelerating flash droughts induced by the joint influence of soil moisture depletion and atmospheric aridity. *Nature Communications*, *13*(1). https://doi.org/10.1038/s41467-022-28752-4

Quan, X. W., Hoerling, M., Smith, L., Perlwitz, J., Zhang, T., Hoell, A., Wolter, K., & Eischeid, J. (2018). 10. Extreme California rains during winter 2015/16: A change in El Niño teleconnection? *Bulletin of the American Meteorological Society*, *99*(1), S49–S53. https://doi.org/10.1175/BAMS-D-17-0118.1

Rajeevan, M., Gadgil, S., & Bhate, J. (2010). Active and break spells of the Indian summer monsoon. *Journal of Earth System Science*, *119*(3), 229–247. https://doi.org/10.1007/s12040-010-0019-4

Svoboda, M., LeComte, D., Hayes, M., Heim, R., Gleason, K., Angel, J., Rippey, B., Tinker, R., Palecki, M., Stooksbury, D., Miskus, D., & Stephens, S. (2002). THE DROUGHT

MONITOR. *Bulletin of the American Meteorological Society*, *83*(8), 1181–1190. https://doi.org/10.1175/1520-0477-83.8.1181

Walker, D. W., Vergopolan, N., Cavalcante, L., Smith, K. H., Agoungbome, S. M. D., Almagro, A., Apurv, T., Dahal, N. M., Hoffmann, D., Singh, V., & Xiang, Z. (2024). Flash Drought Typologies and Societal Impacts: A Worldwide Review of Occurrence, Nomenclature, and Experiences of Local Populations. *Weather, Climate, and Society*, *16*(1), 3–28. https://doi.org/10.1175/WCAS-D-23-0015.1

Wang, L., & Yuan, X. (2018). Two Types of Flash Drought and Their Connections with Seasonal Drought. *Advances in Atmospheric Sciences*, *35*(12), 1478–1490. https://doi.org/10.1007/s00376-018-8047-0

Wang, Y., & Yuan, X. (2022). Land-atmosphere coupling speeds up flash drought onset. *Science of the Total Environment*, *851*. https://doi.org/10.1016/j.scitotenv.2022.158109

Yuan, X., Wang, L., Wu, P., Ji, P., Sheffield, J., & Zhang, M. (2019). Anthropogenic shift towards higher risk of flash drought over China. *Nature Communications*, *10*(1). https://doi.org/10.1038/s41467-019-12692-7